The unusual X-ray emission of the short *Swift* GRB 090515: evidence for the formation of a magnetar?

A. Rowlinson,[1]⋆ P. T. O'Brien,[1] N. R. Tanvir,[1] B. Zhang,[2] P. A. Evans,[1] N. Lyons,[1] A. J. Levan,[3] R. Willingale,[1] K. L. Page,[1] O. Onal,[4] D. N. Burrows,[5] A. P. Beardmore,[1] T. N. Ukwatta,[6,7] E. Berger,[8] J. Hjorth,[9] A. S. Fruchter,[10] R. L. Tunnicliffe,[3] D. B. Fox[5] and A. Cucchiara[5]

[1]*Department of Physics & Astronomy, University of Leicester, University Road, Leicester, LE1 7RH*
[2]*Department of Physics, University of Nevada, 4505 South Maryland Parkway, Las Vegas, NV 89154, USA*
[3]*Department of Physics, University of Warwick, Coventry CV4 7AL*
[4]*Department of Astronomy and Space Sciences, Faculty of Science, Istanbul University, 34119 University, Istanbul, Turkey*
[5]*Department of Astronomy and Astrophysics, Pennsylvania State University, 525 Davey Lab, University Park, PA 16802, USA*
[6]*The George Washington University, Washington, D.C. 20052, USA*
[7]*NASA Goddard Space Flight Centre, Greenbelt, MD 20771, USA*
[8]*Harvard-Smithsonian Center for Astrophysics, 60 Garden Street, Cambridge, MA 02138, USA*
[9]*Dark Cosmology Centre, Niels Bohr Institute, University of Copenhagen, Juliane Maries Vej 30, 2100 Copenhagen, Denmark*
[10]*Space Telescope Science Institute, 3700 San Martin Drive, Baltimore, MD 21218, USA*

ABSTRACT

The majority of short gamma-ray bursts (SGRBs) are thought to originate from the merger of compact binary systems collapsing directly to form a black hole. However, it has been proposed that both SGRBs and long gamma-ray bursts (LGRBs) may, on rare occasions, form an unstable millisecond pulsar (magnetar) prior to final collapse. GRB 090515, detected by the *Swift* satellite was extremely short, with a T_{90} of 0.036 ± 0.016 s, and had a very low fluence of 2×10^{-8} erg cm^{-2} and faint optical afterglow. Despite this, the 0.3–10 keV flux in the first 200 s was the highest observed for an SGRB by the *Swift* X-ray Telescope (XRT). The X-ray light curve showed an unusual plateau and steep decay, becoming undetectable after ∼500 s. This behaviour is similar to that observed in some long bursts proposed to have magnetars contributing to their emission.

In this paper, we present the *Swift* observations of GRB 090515 and compare it to other gamma-ray bursts (GRBs) in the *Swift* sample. Additionally, we present optical observations from Gemini, which detected an afterglow of magnitude 26.4 ± 0.1 at T+ 1.7 h after the burst. We discuss potential causes of the unusual 0.3–10 keV emission and suggest it might be energy injection from an unstable millisecond pulsar. Using the duration and flux of the plateau of GRB 090515, we place constraints on the millisecond pulsar spin period and magnetic field.

Key words: gamma-ray burst: individual: 090515 – stars: neutron.

1 INTRODUCTION

30 yr after the discovery of gamma-ray bursts (GRBs) by the *Vela* satellites (Klebesadel, Strong & Olson 1973), the first X-ray afterglow was detected for GRB 970228 by the *Beppo-SAX* satellite (Costa et al. 1997). With the increased accuracy for the position provided by X-ray afterglows, it was possible to identify the optical afterglow and the host galaxies of many GRBs.

With the launch of the *Swift* satellite (Gehrels et al. 2004), the X-ray afterglow has been studied in great detail, placing tighter constraints on models for GRB emission. Additionally, *Swift* has enabled the detection of short GRB (SGRB) X-ray afterglows, allowing them to be directly compared to long GRB (LGRB) afterglows (Barthelmy et al. 2005a; Gehrels et al. 2005; Hjorth et al. 2005a). Nousek et al. (2006) and Zhang et al. (2006) described the 'canonical GRB light curve' as three stages comprising a steep decline followed by a shallower decay and then a final decay phase. O'Brien et al. (2006) showed that not all X-ray light curves for GRBs are of the 'cannonical' variety. They and Willingale et al.

⋆E-mail: bar7@star.le.ac.uk

(2007) suggested that the X-ray light curve comprises two main components, the prompt emission and the afterglow. The relative strength of these components determines the observed X-ray light curve. A more recent study of all *Swift* X-ray afterglows by Evans et al. (2009) has reinforced these findings. The initial steep decay following the prompt emission typically has a power-law decay with index $\alpha \sim 2$–5, where $f \propto t^{-\alpha}$ (t is the time after the burst in seconds and f is the flux) (O'Brien et al. 2006).

Multiwavelength observations have associated LGRBs with type Ibc core collapse supernovae at cosmological distances (e.g. Hjorth et al. 2003; Stanek et al. 2003), although not all such supernovae produce long GRBs (Woosley & Bloom 2006). The progenitors of SGRBs are less well understood, but the most popular theory is that they originate from the merger of compact binary systems; for example, neutron stars or a neutron star and a black hole (Lattimer & Schramm 1976; Eichler et al. 1989; Narayan, Paczynski & Piran 1992). It has also been suggested that both LGRB and SGRB progenitors could produce an unstable millisecond pulsar. This is expected to contribute a small fraction of the GRB population (Duncan & Thompson 1992; Usov 1992; Dai & Lu 1998a,b; Zhang & Mészáros 2001). Troja et al. (2007) and Lyons et al. (2010) found examples of LGRBs that have an observable plateau and a steep decay in the X-ray light curve, which have been interpreted as caused by energy injection by an unstable millisecond pulsar which then collapses. Magnetar models have also been proposed to explain late central engine activity in SGRBs; for example, late-time plateaus in the X-ray afterglows (Fan & Xu 2006; Dall'Osso et al. 2010; Yu, Cheng & Cao 2010) and X-ray flares (Fan, Zhang & Proga 2005; Gao & Fan 2006). Here we present an analysis of GRB 090515 which is the best case for an early X-ray plateau in an SGRB.

GRB 090515 was one of the shortest GRBs observed by *Swift*, with among the lowest fluence, yet for ∼200 s it had the brightest SGRB X-ray afterglow and did not appear to be fading until a sudden steep decline at ∼240 s. After the first orbit, it was not detected again. Explaining this unusual X-ray behaviour is the subject of this paper. We describe the observations of GRB 090515 in Section 2, compare it to other GRBs in Section 3 and discuss the potential origin of the unusual X-ray emission in Section 4. Throughout the paper we adopt a cosmology with $H_0 = 71$ km s^{-1} Mpc^{-1}, $\Omega_m = 0.27$, $\Omega_\Lambda = 0.73$. Errors are quoted at 90 per cent confidence for X-ray data and at 1σ for optical data.

2 OBSERVATIONS

2.1 *Swift* observations

All analyses have been performed by using standard routines in HEASOFT, XSPEC, QDP and the automatic X-ray Telescope (XRT, Burrows et al. 2005) data products produced by the UK Swift Science Data Centre (Evans et al. 2007, 2009).

Swift triggered on GRB 090515 at 04:45:09 UT on 2009 May 15 with BAT position RA = 10^{h}56^{m}41^s and Dec. = +14°27′22″ (Beardmore et al. 2009). The Ultra-Violet and Optical Telescope (UVOT) enhanced refined XRT position was RA = 10^{h}56^{m}36^{s}11 and Dec. = +14°26′30″3 with an uncertainty of 2.7 arcsec (Osborne et al. 2009).

The T_{90} duration of GRB 090515 was 0.036 ± 0.016 s (Barthelmy et al. 2009a). The spectrum of the prompt gamma-ray emission can be fitted by a single power law, of photon index $\Gamma_\gamma = 1.6 \pm 0.2$ (Barthelmy et al. 2009a). The fluence is $2.0 \pm 0.8 \times 10^{-8}$ erg cm^{-2} and the peak photon flux is 5.7 ± 0.9 ph cm^{-2} s^{-1}. All values are
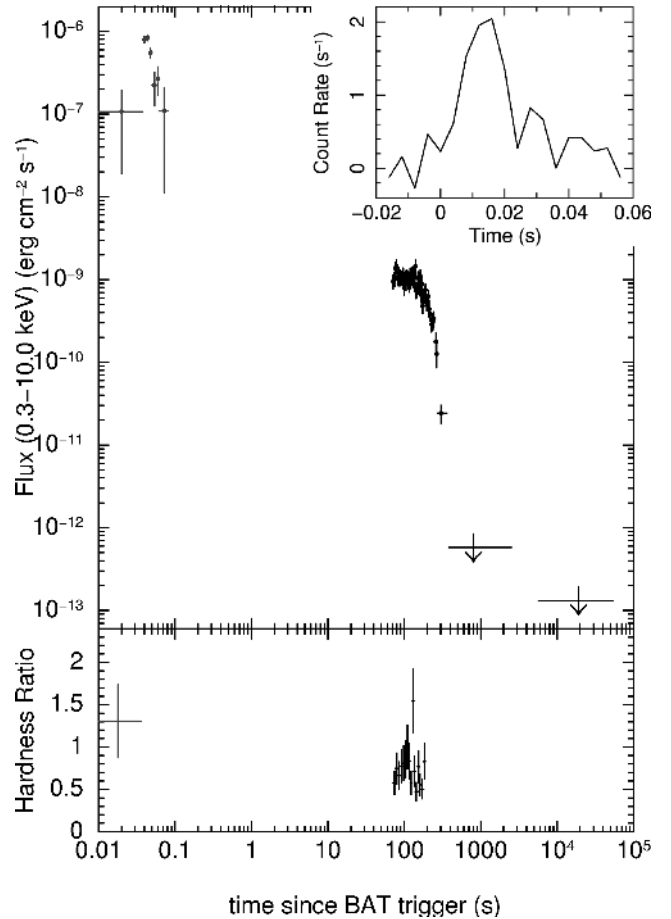

Figure 1. The combined light curve for GRB 090515, in grey are the BAT data and in black are the XRT data. In the lower box there is the hardness ratio for the BAT data ((50–100) keV/(25–50) keV) in grey and the hardness ratio for the XRT data ((1.5–10) keV/(0.3–1.5) keV) in black. Inset is the BAT count rate per detector light curve with linear time.

in the 15–150 keV energy band. The BAT light curve is shown in Fig. 1 as the grey data points and also shown in the inset with linear time. The BAT count rates were converted to flux in the energy band 0.3–10 keV using the average spectral index for the BAT and the XRT spectra. There is no evidence of extended emission detected in the BAT energy range (Norris, Gehrels & Scargle 2010).

We completed a spectral lag analysis for GRB 090515 using the cross-correlation function method described in Ukwatta et al. (2010), the 8 ms time binned light curve and BAT channels 1, 2 and 3. Channel 4 did not detect enough emission to make a lag measurement. The lag times are (with 1σ errors): lag (Ch 2 − Ch 1) = 6 ± 4 ms, lag (Ch 3 − Ch 2) = 3 ± 2 ms and lag (Ch 2 − Ch 1) = 10 ± 4 ms. Typically, SGRBs have negligible lag times (Norris & Bonnell 2006; Yi et al. 2006) and LGRBs have typical lag times ranging from 20 to ∼1000 ms (Ukwatta et al. 2010), so it is interesting that GRB 090515 appears to have a small lag time.

The X-ray spectrum in the 0.3–10 keV energy band is best fitted by an absorbed power law with $\Gamma_X = 1.88 \pm 0.14$ and $N_H = 6.1^{+3.0}_{-2.8} \times 10^{20}$ cm^{-2}, in excess of the Galactic $N_H = 1.9 \times 10^{20}$ cm^{-2} (Beardmore & Evans 2009). The X-ray light curve is best fitted by a broken power law with two breaks giving a reduced χ^2_ν of 0.86. The initial decay is relatively flat ($\alpha_1 = 0.29^{+0.08}_{-0.27}$) with a break at $T_1 = 156.2^{+9.3}_{-26.2}$s followed by a steeper decay of $\alpha_2 = 2.51^{+0.38}_{-0.70}$. At $T_2 = 240.8^{+7.4}_{-9.8}$s it breaks to an extremely steep decay of $\alpha_3 > 9$.

Table 1. The optical observations of the field of GRB 090515.

Telescope	Mid-point time after trigger (s)	Exposure time	Band	Upper limit (mag)	Flux upper limit (erg cm^{-2} s^{-1} Hz^{-1})
KAIT	20	540	*R*	19.1[1]	6.6×10^{-28}
Super LOTIS	43	10	*R*	17.7[2]	2.4×10^{-27}
ROTSE III	86	67	*R*	18.4[3]	1.3×10^{-27}
UVOT	142	146	White	20.35[4]	2.1×10^{-28}
UVOT	1228	488	White	21.24[4]	9.2×10^{-29}
KAIT	2078	540	*R*	20.5[1]	1.8×10^{-28}
Lick	2286	60	*R*	21.3[5]	8.7×10^{-29}
ROVOR	5496	4200	*R*	21.4[6]	7.9×10^{-29}

[1] Li, Chornock & Filippenko (2009), [2] Williams, Updike & Milne (2009), [3] Rujopakarn, Schaefer & Rykoff (2009), [4] Seigel & Beardmore (2009), [5] Perley, Kislak & Ganeshalingam (2009b), [6] Pace, Pearson & Ward Moody (2009).

Table 2. Log of Gemini observations.

Epoch	Date start (UT)	Start time after trigger (s)	Exposure time (s)	Filter	Seeing (arcsec)	Airmass	Magnitude	Flux (erg cm^{-2} s^{-1} Hz^{-1})
1	May 15 06:27	$\sim$6100	1800	r	0.5	1.021	26.36 ± 0.12	8.2×10^{-31}
2	May 16 05:44	$\sim 9 \times 10^4$	1800	r	1	1.005	26.54 ± 0.33	6.95×10^{-31}
3	November 28 14:20	$\sim 1.6 \times 10^7$	2800	r	0.8	1.226	>27.4	$<4.55 \times 10^{-31}$

Although, we have fitted the X-ray light curve using a broken power law, we note that the decay appears to be a smooth curve. The X-ray light curve is shown in Fig. 1 as the black data points and the lower panel shows the hardness ratio for the gamma-ray emission (in grey), i.e. the ratio of the 50–100 keV emission to the 25–50 keV emission, and the hardness ratio of the X-ray emission [in black, (1.5–10) keV/(0.3–1.5) keV]. The hardness ratio is fairly constant during the plateau, with the exception of a point at $\sim$120 s that could be a flare and does correspond to a small peak in the X-ray light curve, but this may just be noise. There are insufficient counts to characterize the hardness ratio during the decay.

2.2 Early optical observations

The field of GRB 090515 was observed at early times by several optical telescopes but none detected an optical afterglow. The upper limits of the *R* band and white filter observations are given in Table 1. During the plateau phase, we can predict the optical flux density, assuming that the X-ray and optical emission are from the same emitting region. If there is not a cooling break in the spectrum (i.e. $\Gamma_X = \Gamma_{OX}$) then we would expect the optical flux to be 1.7×10^{-26} erg cm^{-2} s^{-1} Hz^{-1}, corresponding to an apparent magnitude of $R = 15.6$. This is brighter than all of the optical upper limits during the plateau, so we should have observed the optical afterglow. However, if there were a cooling break in the spectrum between optical and X-ray then $\Gamma_{OX} = \Gamma_X - 0.5$ and, in this case, the optical flux density would be 8.7×10^{-29} erg cm^{-2} s^{-1} keV^{-1} Hz^{-1}, corresponding to an apparent magnitude of $R = 21.3$. This is slightly deeper than the optical upper limit provided by UVOT. Therefore, if the optical emission was from the same emitting region as the X-ray and there is a cooling break in the spectrum, there is a slim chance that the optical flux was below the observed limits so the non-detection is consistent with the X-ray data.

2.3 Gemini observations

We obtained optical observations of GRB 090515 using Gemini North and GMOS beginning at 06:26 UT, approximately 1.7 h after the burst, with a second epoch observation being taken on the subsequent night, and a final comparison epoch on 2009 November 28. The images were obtained in the *r*-band, and were reduced via the standard IRAF Gemini tasks (Tody 1993). The image conditions for our first epoch were excellent, with seeing of 0.5 arcsec, resulting in extremely deep imaging in our total exposure time of 1800 s. A full log of observations is shown in Table 2.

Within the refined XRT error circle we locate a single source at RA $= 10^h 56^m 35^s.89$ and Dec. $= +14°26'30''.0$, with a magnitude of $r = 26.36 \pm 0.12$, calibrated against existing Sloan Digital Sky Survey (SDSS) observations of the field, shown in Fig. 2. This source is still visible, but at lower significance in our shallower images obtained on 16 May ($r = 26.54 \pm 0.33$). In our final epoch there is no source visible at the afterglow location, to a limiting magnitude of $r > 27.4$ confirming a fading counterpart. We therefore conclude that this is the optical afterglow of GRB 090515. At $r = 26.36$, this is the faintest GRB afterglow ever discovered at similar
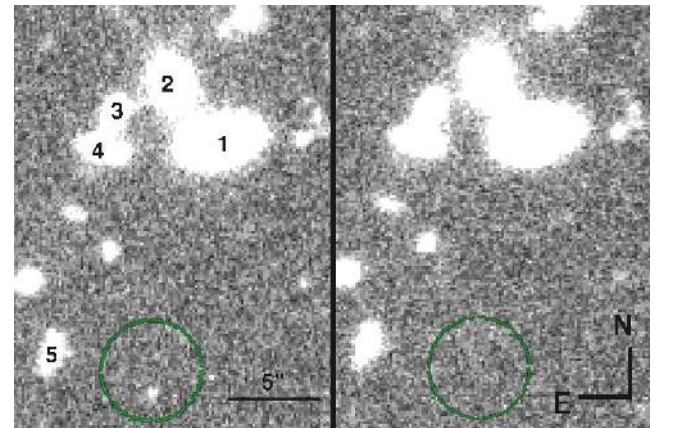

Figure 2. The circle marks the location of the XRT enhanced position of GRB 090515 on the Gemini observation from epoch 1 on the left and epoch 3 on the right. An optical afterglow candidate is observed within the error circle. Labelled are the brightest nearby galaxies.

Table 3. Photometry of the nearby galaxies, as labelled in Fig. 2, calibrated using SDSS observations.

Galaxy	Magnitude	Offset (arcsec)
1	20.2 ± 0.1	14
2	21.3 ± 0.1	16
3	22.5 ± 0.1	15
4	22.6 ± 0.1	13
5	23.4 ± 0.1	6

times after the burst, and confirms the necessity of rapid and deep observations with 8-m class observatories. As the observed X-ray absorption is relatively low ($N_H \sim 6 \times 10^{20}$ cm^{-2}), the faint optical afterglow is unlikely to be a consequence of extinction (unless it is at high redshift). The optical afterglow has a relatively flat light curve, with a decay slope of $0.06^{+0.32}_{-0.19}$.

Comparing this afterglow to the sample in Nysewander, Fruchter & Pe'er (2009), we note that this is the first SGRB with a fluence below 10^{-7} erg cm^{-2} with a detected optical afterglow. Additionally, the afterglow at 1.7 h is fainter than all the observed optical afterglows at 11 h. GRB 080503 also had an initially very faint optical afterglow, but it then rebrightened to a peak of $r \sim 25.5$ at 1 d and no host galaxy was identified (Perley et al. 2009a).

Assuming there is not a cooling break in the spectrum, i.e. $\Gamma_X = \Gamma_{OX}$, we predict that the X-ray flux, 0.3–10 keV, at the time of the optical observations should be 6.6×10^{-15} erg cm^{-2} s^{-1}. This is consistent with the observed upper limit.

Labelled in Fig. 2 are the five brightest nearby galaxies and Table 3 provides their magnitudes and offsets from the GRB location. These galaxies are candidates for the host galaxy of GRB 090515, with significant offsets, or the burst could be associated with a significantly fainter underlying host galaxy.

3 COMPARISON TO OTHER GRBS

The XRT light curve of the low fluence GRB 090515 is unusual as it goes from being the brightest SGRB in X-rays to one of the faintest within seconds. The fluence in X-rays during the plateau is significantly higher than the fluence in gamma-rays. Additionally, the final decay is the steepest decay observed to date (Evans et al. 2009). The X-ray spectral index of GRB 090515 is not unusual compared to other SGRBs. In Table 4, we provide a summary of the properties of the long and short GRBs to which we compare GRB 090515 in detail.

In Fig. 3, we show the 15–150 keV fluence and 0.3–10 keV flux at $t_0 + 100$ s for all the SGRBs in the *Swift* sample with $T_{90} \leq 2$ s and which were observed by XRT at this time. GRB 090515 is shown with a filled circle. As expected, the higher-fluence GRBs tend to have higher-flux X-ray afterglows. GRB 090515 is an exception to this alongside GRB 070724A; both of these bursts have an unusually high initial X-ray flux for their fluence. In Fig. 5(a), we compare the combined BAT-XRT light curves of GRB 090515 and GRB 070724A. The initial XRT flux of 070724A appears to be consistent with flares (as there is a varying hardness ratio) and an underlying broken power-law decay. There is no obvious plateau phase for GRB 070724A, but this may have occurred prior to the XRT observations. The steep decay phase of GRB 070724A, with $\alpha = 3.44^{+0.60}_{-0.35}$ is much shallower than the steep decay of GRB 090515. Additionally, the optical afterglow of GRB 070724A had a magnitude of $i = 23.79 \pm 0.07$ at 2.3 h after the burst, corresponding

Table 4. The GRBs considered in detail in this paper.

GRB	T_{90} (s)	Γ (15–150 keV)	Fluence (15–150 keV) (10^{-8} erg cm^{-2})
090515	0.036 ± 0.016	1.6 ± 0.2	2.0 ± 0.8[1],[2]
090607	2.3 ± 0.1	1.25 ± 0.30	11 ± 2[3]
080520A	2.8 ± 0.7	2.90 ± 0.51	5.5 ± 1.4[4]
080503	170 ± 20	2.00 ± 0.13	200 ± 10[5]
070724A	0.4 ± 0.04	1.81 ± 0.33	3.0 ± 0.7[6]
070616	402 ± 10	1.61 ± 0.04	1920 ± 30[7]
070209	0.10 ± 0.02	1.55 ± 0.39	1.1 ± 0.3[8]
060717	3.0 ± 1	1.72 ± 0.38	6.5 ± 1.6[9]
051221B	61 ± 1	1.48 ± 0.18	113 ± 13[10]
051105	0.028 ± 0.004	1.33 ± 0.35	2.0 ± 0.46[11]
050813	0.6 ± 0.1	1.19 ± 0.33	4.4 ± 1.1[12]
050509B	0.048 ± 0.022	1.5 ± 0.4	0.78 ± 0.22[13]
050421	10.3 ± 2	1.7 ± 0.4	8.8 ± 2.9[14]

[1] Barthelmy et al. (2009a) [2] Sakamoto & Beardmore (2009) [3] Barthelmy et al. (2009b) [4] Sakamoto et al. (2008) [5] Ukwatta et al. (2008) [6] Parsons et al. (2007) [7] Sato & Barthelmy (2007) [8] Sakamoto et al. (2007) [9] Markwardt et al. (2006) [10] Fenimore et al. (2005) [11] Barbier et al. (2005) [12] Sato et al. (2005) [13] Barthelmy et al. (2005b) [14] Sakamoto et al. (2005).
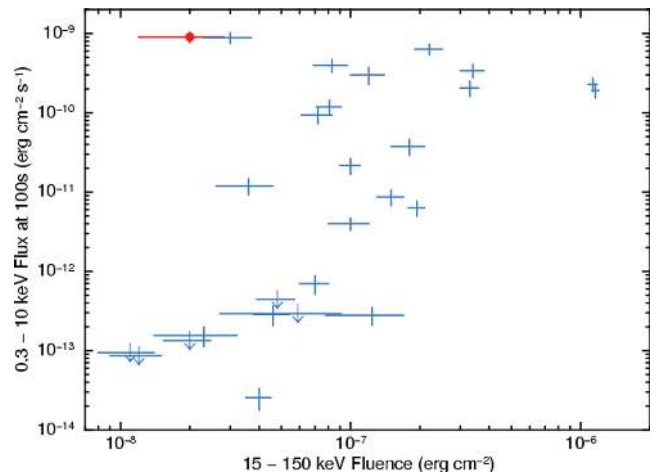
Figure 3. The fluence in the energy band 0.3–10 keV versus the 15–150 keV flux for all *Swift* SGRBs which were observed at 100 s after the trigger time. The filled circle marks the location of GRB 090515.

to a flux of 6.86×10^{-30} erg cm^{-2} s^{-1} Hz^{-1}, with an associated host galaxy (Berger et al. 2009; Kocevski et al. 2010). This flux is almost an order of magnitude larger than the optical afterglow of GRB 090515 at 1.7 h and GRB 090515 does not have an identified host galaxy. However, GRB 070724A does share many similarities with GRB 090515, so we cannot rule out the possibility that they originate from a similar progenitor.

Fig. 4(a) shows the light curves for the observed *R*-band optical afterglows associated with SGRBs (published values converted from magnitudes into flux density in Jy), GRB 090515 is the faintest observed and one of the earliest detections after the trigger time. In Fig. 4(b) we have divided the optical fluxes by the XRT flux at 1000 s after the trigger time. When we have considered the XRT flux at 1000 s, the optical afterglow of GRB 090515 is not unusually faint compared to other SGRBs. We also show the optical light curve for GRB 080503 (a short burst with extended emission Perley et al. 2009a) in Fig. 4(c) in comparison to GRB 090515.
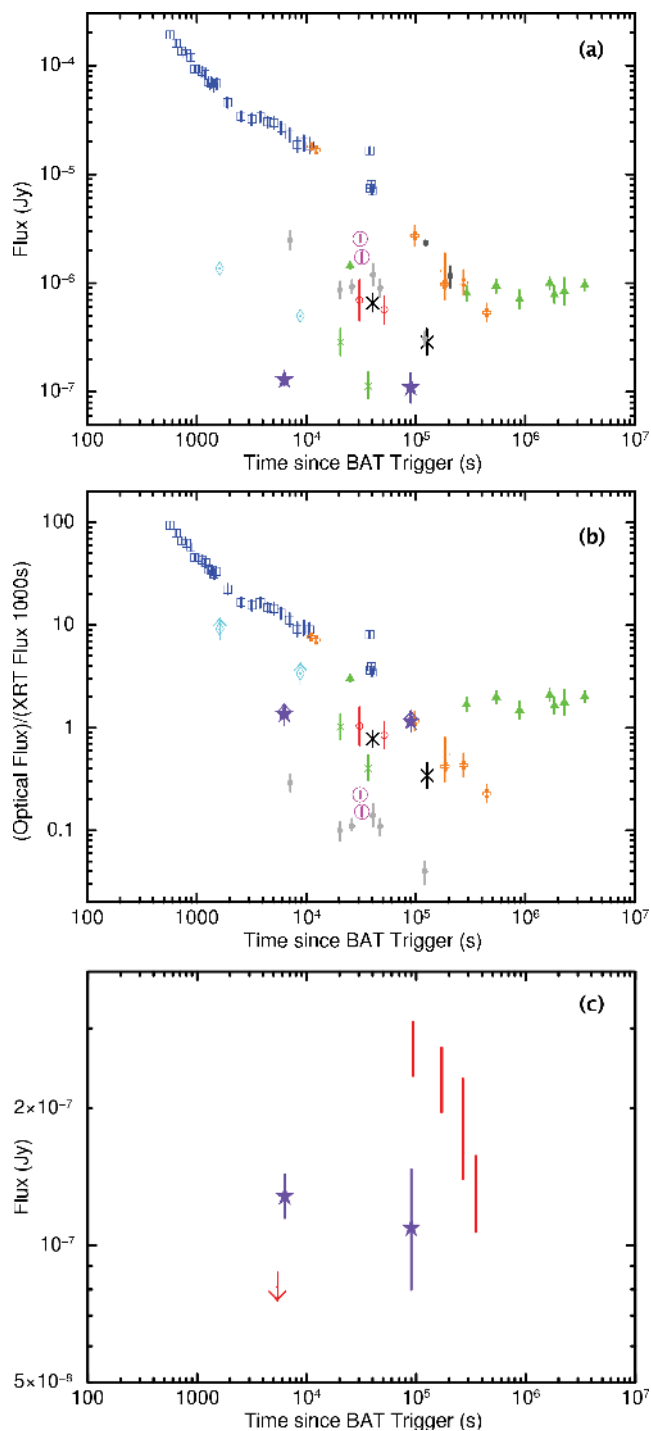
3.1 GRBs with similar fluence to GRB 090515

As the fluence of GRB 090515 in the 15–150 keV energy band was one of the lowest fluences observed for SGRBs, here we compare it to other low-fluence GRBs.

GRB 050509B and GRB 050813 were short GRBs detected by the *Swift* satellite that were similar to GRB 090515 during the prompt emission phase. However, the combined BAT and XRT light curves for GRBs 050509B and 050813, shown in Fig. 5(b), do not show the same X-ray plateau extending to ~200 s after the burst. GRBs 050509B and 050813 have both been used to place constraints on the compact binary merger model of SGRBs (Gehrels et al. 2005; Hjorth et al. 2005b; Bloom et al. 2006; Ferrero et al. 2007). The observed upper limits for GRB 090515 at late times (after 400 s) are consistent with the later emission observed for GRBs 050509B and 050813. This suggests that the plateau and steep decay are an additional component in the light curve of GRB 090515.

GRB 051105 is an SGRB with a fluence identical to that of GRB 090515, but its afterglow was undetectable by XRT in observations starting 68 s after the burst (Mineo et al. 2005a). GRB 070209 had the lowest SGRB fluence and was also undetectable by XRT in observations starting 78 s after the burst (Sato et al. 2007).

In Fig. 5(c), the X-ray light curve of GRB 090515 is compared to the two lowest-fluence LGRBs in the *Swift* sample which were detected by XRT. These are GRB 080520A and GRB 060717A, they both have significantly higher fluence in the 15–150 keV band than GRB 090515 (due to having longer durations), but are a lot fainter in X-rays, again suggesting additional X-ray emission in GRB 090515.

It is possible that these GRBs had plateau phases which end prior to the XRT observations. However, as *Swift* slewed promptly to these GRBs (observations typically starting within 100 s), a plateau phase would need to be significantly shorter than that observed for GRB 090515. The main exception to this is GRB 060717A, which had XRT observations beginning when GRB 090515 was in the steep decay phase.

3.2 GRBs with steep decays

The GRB with an X-ray light curve most similar to GRB 090515 is GRB 090607, which has a T_{90} just above the short-long boundary. They are compared in Fig. 5(d). Both light curves show a distinctive steep decay at ~200 s. However, the emission of GRB 090607 between 80 and 100 s is not a plateau as observed in GRB 090515 and, given the hard spectrum which softens as the emission decays (shown in the lower panel of Fig. 5d), is more likely due to a flare at the start of the XRT observations.

4 DISCUSSION

The steep decay in the unusual X-ray light curve of GRB 090515 cannot be explained using the external shock afterglow models. Instead, we consider if this GRB was a naked burst with faint, rapidly fading emission, and if the X-ray plateau is powered by an unstable millisecond pulsar. These possibilities are discussed below.

4.1 An underluminous naked LGRB

If a GRB occurs in a very low density ISM then the afterglow from external shocks between the jet and the ISM could be too faint for
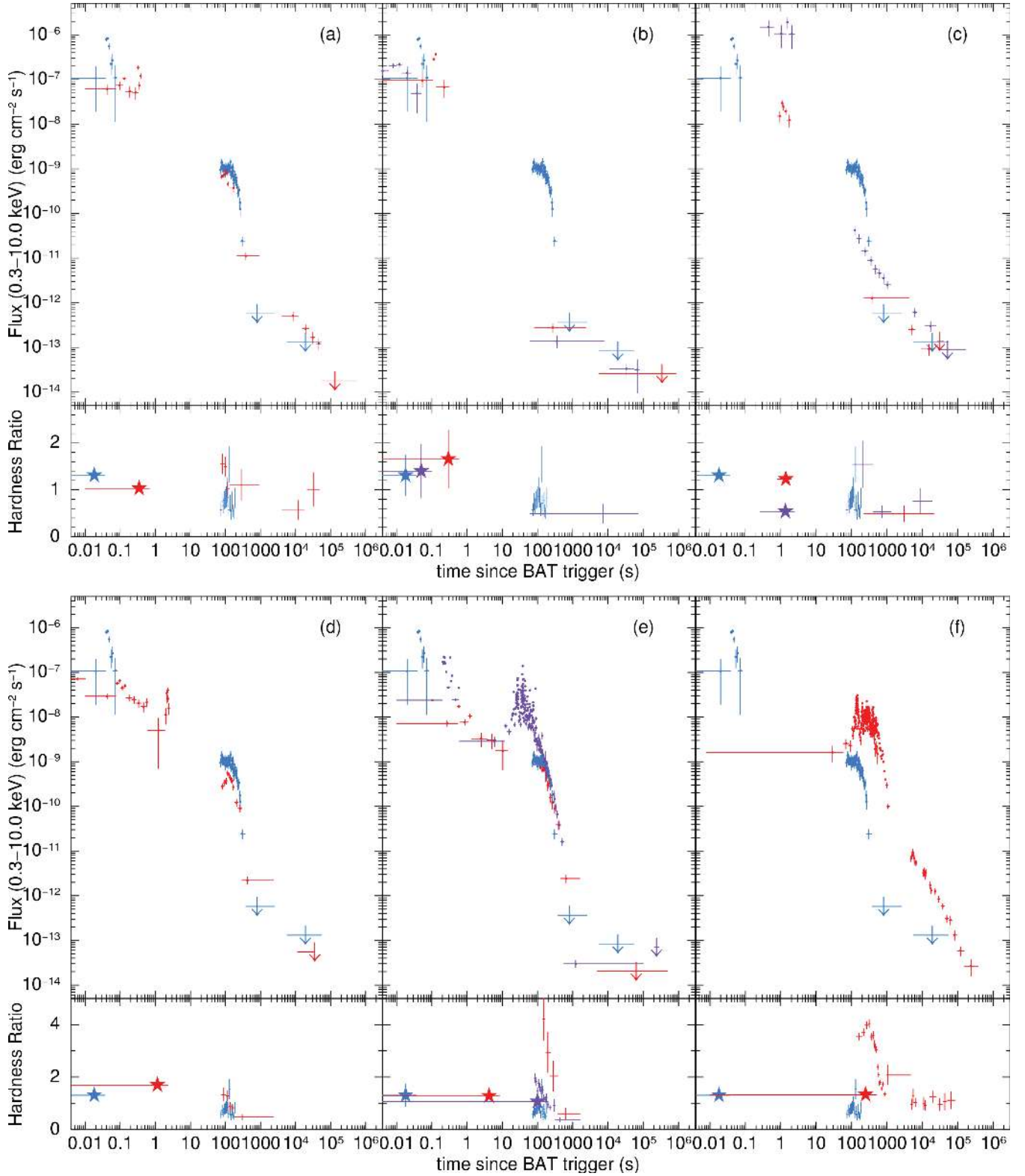
Figure 4. (a) The optical flux light curves for all observed SGRB afterglows in the *R* band. (b) Normalized using the XRT flux at 1000 s. Colour scheme: GRB 090515, purple star; GRB 091109B, small green X (Levan et al. 2009; Malesani et al. 2009); GRB 090426, dark blue open square (Antonelli et al. 2009; Xin et al. 2010); GRB 090305, light blue open diamond (Cenko et al. 2009; Berger & Kelson 2009); GRB 080905A, small red open circle (Rowlinson et al. 2010); GRB 071227, green filled triangle (Berger, Morrell & Roth 2007); GRB 070809, large black X (Perley, Thoene & Bloom 2007; Perley et al. 2008); GRB 061201, large pink open circle (Stratta et al. 2007); GRB 060121, dark grey filled circle (Levan et al. 2006); GRB 051221A, orange open cross (Soderberg et al. 2006); GRB 050709, light grey filled square (Hjorth et al. 2005a). (c) The optical flux light curve for GRB 090515 (purple stars) with GRB 080503 (red).

Figure 5. The BAT-XRT light curve and hardness ratios for GRB 090515 in blue in comparison to other GRBs. (a) GRB 070724A in red. (b) GRB 050813 in red and GRB 050509B in purple. (c) GRB 060717A in red and GRB 080520A in purple. (d) GRB 090607 in red. (e) GRB 050421 in red and GRB 080503 in purple. (f) GRB 070616 in red. In the lower boxes for each graph, there is the hardness ratio for the BAT data [(50–100) keV/(25–50) keV], with a star, and the hardness ratio for the XRT data [(1.5–10) keV/(0.3–1.5) keV].

detection by *Swift*. Instead, there would just be the prompt emission followed by a rapid decline due to the 'curvature effect' (Kumar & Panaitescu 2000). This predicts a decay in flux described by

$$f_\nu \propto \nu^{-\beta} t^{-2-\beta}, \qquad (1)$$

where β is the observed spectral energy index at frequency ν ($\beta = \Gamma - 1$), and t is the time since the trigger. We should observe a decay $\alpha = 2 + \beta = \Gamma + 1$. We compare here GRB 090515 with a good candidate for a naked burst, GRB 050421 (Godet et al. 2006).

GRB 050421 was a weak, long GRB detected by BAT following a steep decay, as shown in Fig. 5(e), although the decay is not as steep as for GRB 090515. There is evidence of spectral evolution, as the emission is getting softer [the lower panel of Fig. 5(e)]; however, the spectral evolution is during the steep decay and not the plateau region. The initial hardness ratio for (1.5–10) keV/(0.3–1.5) keV is six times larger for GRB 050421 than GRB 090515. Godet et al. (2006) explained the steep decay ($\alpha = 3.1 \pm 0.1$) of GRB 050421 by assuming it was a 'naked burst', i.e. there was no forward shock component of the afterglow as the interstellar medium (ISM) was not dense enough for the shock wave to produce a typical afterglow. The detected decaying emission is consistent with the 'curvature effect'. GRB 080503, shown in Fig. 5(e), has also been explained as a short 'naked burst' with extended emission detected in the BAT (although not a plateau), the X-ray decay is consistent with the 'curvature effect' (Perley et al. 2009a). However, the steep decay for both of these are significantly shallower than the decay of GRB 090515, which was $\alpha_3 > 9$ (with t_0 at the start of the prompt emission).

GRB 090515 shares some similarities with GRB 050421 and GRB 080503 (Godet et al. 2006; Perley et al. 2009a). Zhang et al. (2009) suggested that the burst duration, observed by BAT, represents the duration that the jet is relativistic and, with a non-relativistic (or less relativistic) jet, the central engine can be active for longer than this time and may be observed by XRT. Therefore, the X-ray plateau observed for GRB 090515 could be a continuation of the prompt emission, which has fallen below the threshold of BAT. So with a more sensitive detector, GRB 090515 may have been identified as an LGRB. If true, we should expect to see that the steep decay matches the 'curvature effect' like GRB 050421. During the plateau, the spectral index Γ_x is 1.88 ± 0.14 predicting a steep decay slope of $\alpha = 2.88 \pm 0.14$. As the observed decay is significantly steeper than this, it does not fit the 'curvature effect' theory. Using the method described by Liang et al. (2006), we shifted the t_0 to the possible flare at the end of the plateau in GRB 090515. The steep decay becomes less extreme, $\alpha = 3.7 \pm 0.6$, but still steeper than the predicted decay slope. This method relies on correctly identifying the time at which the central engine is last active and with a plateau in the light curve this point is difficult to identify. The steep decay of GRB 090515 following the plateau may be consistent with the 'curvature effect' if a later location of t_0 is identified. Alternatively, this could be associated with a narrow opening angle for the jet which creates the plateau, as in that case outside of $1/\Gamma$ there would be very little high-latitude emission, giving a much steeper decay slope. It is also possible that the spectrum softens immediately prior to the steep decay; however, we do not have enough observed counts to produce a reliable X-ray spectrum at this time.

GRB 090515 can potentially be explained as an underluminous naked long GRB; however, this is reliant on the assumption that the plateau is powered by prolonged activity in the central engine.

4.2 An unstable millisecond pulsar (magnetar) central engine

The bright X-ray plateau in the light curve of GRB 090515 could be associated with the formation, emission and collapse of a millisecond pulsar. There have been predictions that in some GRBs an unstable millisecond pulsar may be formed (Duncan & Thompson 1992; Usov 1992; Dai & Lu 1998a,b; Zhang & Mészáros 2001). At formation, there is enough rotational energy to prevent gravitational collapse. This energy can be released as electromagnetic radiation or gravitational waves, causing the pulsar to spin down until it reaches a critical point at which it is no longer able to support itself. At this point the pulsar collapses to a black hole and the emission stops. This would be evident in the X-ray light curve as a plateau caused by energy injection from the millisecond pulsar followed by an extremely steep decay when the pulsar collapses. We might expect millisecond pulsars formed during the core collapse of a massive progenitor star to be associated with long GRBs and this has been suggested by Troja et al. (2007) and Lyons et al. (2010). GRB 090515 was an extremely short GRB, but a millisecond pulsar could be formed by two merging neutron stars (a potential progenitor of SGRBs), depending on various assumptions about the neutron stars' equations of state (Dai & Lu 1998a; Dai et al. 2006; Yu & Huang 2007).

Troja et al. (2007) and Lyons et al. (2010) studied LGRBs with a plateau and a steep decay and GRB 090515 shows similarities to them. In Fig. 5(f), we compare the light curve of GRB 090515 to that of GRB 070616 (Starling et al. 2008), one of the samples chosen by Lyons et al. (2010) as potentially showing evidence of an unstable millisecond pulsar. When comparing the light curves, GRB 070616 appears to be a brighter and longer version of GRB 090515 but with a bright afterglow component at later times.

We have used the following equations from Zhang & Mészáros (2001) (equations 2 and 3) to determine if GRB 090515 could be a millisecond pulsar, using $T_{em,3}$, the rest-frame duration of the plateau in units of 10^3 s, and $L_{em,49}$, the luminosity of the plateau in units of 10^{49} erg s^{-1}, in the rest-frame energy band 1–1000 keV. The equations are rearranged to give equations (4) and (5); these are used to predict the magnetic field strength and the spin period of a pulsar formed by this method:

$$T_{em,3} = 2.05 \left(I_{45} B_{p,15}^{-2} P_{0,-3}^2 R_6^{-6} \right), \qquad (2)$$

$$L_{em,49} \sim \left(B_{p,15}^2 P_{0,-3}^{-4} R_6^6 \right), \qquad (3)$$

$$B_{p,15}^2 = 4.2025 I_{45}^2 R_6^{-6} L_{em,49}^{-1} T_{em,3}^{-2}, \qquad (4)$$

$$P_{0,-3}^2 = 2.05 I_{45} L_{em,49}^{-1} T_{em,3}^{-1}, \qquad (5)$$

where I_{45} is the moment of inertia in units of 10^{45} g cm^2, $B_{p,15}$ is the magnetic field strength at the poles in units of 10^{15} G, R_6 is the radius of the neutron star in 10^6 cm and $P_{0,-3}$ is the initial period of the compact object in milliseconds. These equations apply to the electromagnetic-dominated spin-down regime, as the gravitational wave-dominated regime would be extremely rapid and produce a negligible effect in our analysis. We could assume, as in Lyons et al. (2010), that we can use standard values for a neutron star so that $I_{45} \sim 1$ and $R_6 \sim 1$ which may be appropriate for a collapsar. However, as we would be forming an unstable millisecond pulsar by merging two neutron stars the true values may be different, depending on the mass and equation of state. For a millisecond pulsar formed by a binary merger, we can take the mass of the neutron star to be $M_{NS} = 2.1$ M$_\odot$ (Nice et al. 2005) and estimate $I_{45} \sim 1.5$.

Although GRB 090515 has many properties similar to other SGRBs suggesting the progenitor is most likely a compact binary merger, there have been predictions that collapsars may also produce an SGRB (for example, from an orphan precursor jet, Janiuk, Moderski & Proga 2008) and evidence that a significant fraction of SGRBs are related to collapsars rather than compact binary mergers (Virgili et al. 2009; Cui, Aoi & Nagataki 2010). So in the following analysis we compare both progenitor models.

As a redshift was not obtained for this GRB, we used a range of redshifts from $z = 0.2$ up to an upper limit of $z = 5.0$ consistent with the detection of the optical afterglow. We assume that the millisecond pulsar was formed at $t \sim 0$ and, hence, the duration of the plateau in the observer frame is 240 s. We calculate the luminosity of the plateau using the observed 0.3–10 keV flux of $\sim 1 \times 10^{-9}$ erg cm^{-2} s^{-1}, the spectral index during the plateau (1.88) and a k-correction (Bloom, Frail & Sari 2001). These values were then substituted into equations (4) and (5) to calculate $B_{p,15}$ and $P_{0,-3}$. These are plotted as a blue contour in Fig. 6(a) assuming it was formed from a collapsar and a purple contour if formed by a binary neutron star merger.

Also shown in Fig. 6(a), are the regions in which a millisecond pulsar would be expected, as defined in Lyons et al. (2010): the red line represents the breakup spin-period for a neutron star of mass 1.4 M$_\odot$ (≥ 0.96 ms, Lattimer & Prakash 2004). Using equation (6) (Lattimer & Prakash 2004), we calculate this limit for the binary merger scenario with a mass of 2.1 M$_\odot$ to be $P \geq 0.66$ ms (where P is the minimum spin period of the neutron star in ms) and this is shown with a red dashed line:

$$P_{0,-3} \geq 0.81 M_{1.4}^{-1/2} R_6^{3/2} \text{ ms.} \tag{6}$$

The initial rotation period needs to be ≤ 10 ms (Usov 1992) and the lower limit for the magnetic field is $\geq 10^{15}$ G (Thompson 2007). This shows that GRB 090515 could have formed a millisecond pulsar if it had a redshift of $0.3 < z < 3.5$ for a collapsar progenitor or a redshift of $0.2 < z < 4.4$ for a binary merger progenitor. These are both very reasonable redshift ranges when we compare them to the sample of GRBs. The magnetic field for a given spin period is slightly lower for a binary merger progenitor than for a collapsar progenitor. Alongside the prediction by Troja et al. (2007) and Lyons et al. (2010) of a plateau followed by a steep decay for the light curve of a millisecond pulsar collapsing to a black hole, which matches the observed light curve for GRB 090515, this analysis provides a consistent case for GRB 090515 forming a millisecond pulsar irrespective of the two initial progenitor models considered.

Using a causality argument, i.e. that the speed of sound on the neutron star cannot exceed the speed of light, we can place a tighter constraint on the minimum possible radius, R_6 and $M_{1.4}$, where $M_{1.4}$ is the mass of the neutron star in 1.4 M$_\odot$, using equation (7) (Lattimer et al. 1990). The moment of inertia, given in equation (8), is based on the assumption that the neutron star can be modelled as an uniform sphere

$$R_6 > 0.6225 M_{1.4}, \tag{7}$$

$$I_{45} \sim M_{1.4} R_6^2. \tag{8}$$

This constraint on radius and moment of inertia for a given mass can be substituted into equations (4) and (5) to define a forbidden region for a given neutron star mass, plateau duration and luminosity. The forbidden region is described by equations (9) and (10) and is shown in Fig. 6(b) for GRB 090515 assuming a mass of 1.4 M$_\odot$, for a collapsar progenitor (red curved line), and 2.1 M$_\odot$,
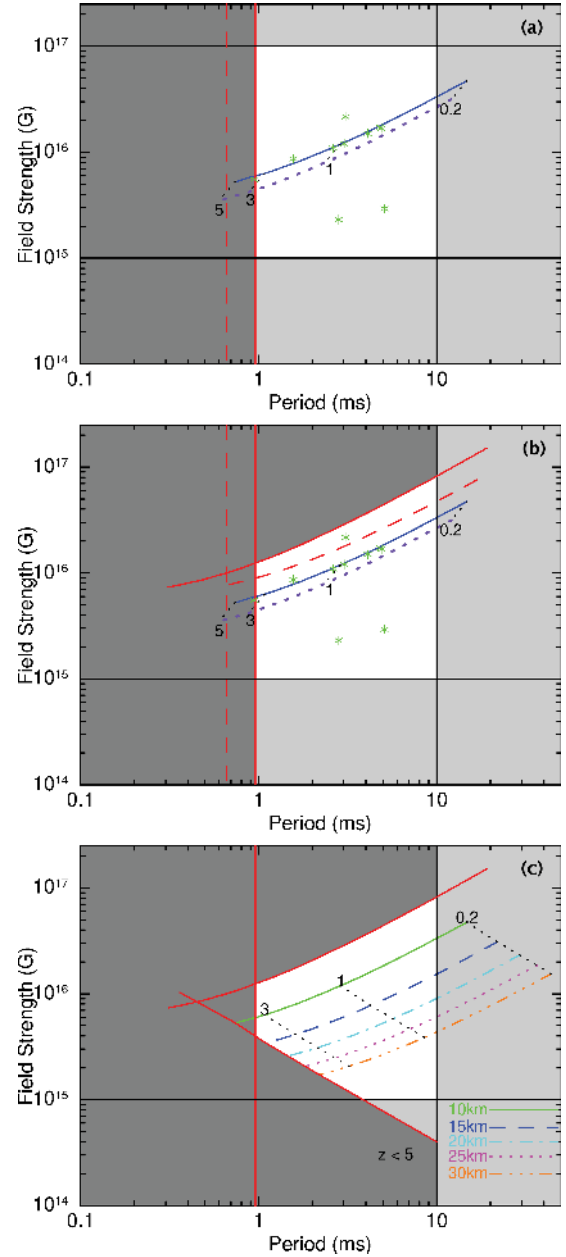

Figure 6. (a) The blue line shows the magnetic field and period for a millisecond pulsar formed during GRB 090515 as a function of redshift assuming a neutron star mass of 1.4 M$_\odot$ and the purple dotted line assumes a neutron star mass of 2.1 M$_\odot$. The green stars are the 18° beamed LGRB sample from Lyons et al. (2010). The red line shows the limit at which the progenitor would violate the breakup spin period of a pulsar for a mass of 1.4 M$_\odot$ and the dashed red line is for a mass of 2.1 M$_\odot$. The other regions are as defined in Lyons et al. (2010); dark grey shading corresponds to forbidden regions (assuming a mass of 1.4 M$_\odot$) and light grey are limits based on the previous studies (as discussed in the text). The dotted lines represent contours of equal redshift decreasing from left to right. (b) The upper magnetic field limit in (a) has been replaced by the red curved line giving the forbidden region assuming causality shaded in dark grey (assuming a mass of 1.4 M$_\odot$). This region will change depending on the mass of the neutron star, the rest-frame duration and luminosity of the plateau. The red dashed curved line represents the forbidden region for a binary merger progenitor. (c) The different contours represent the effect of increasing the radius of the neutron star from 10 to 30 km assuming a constant mass of 1.4 M$_\odot$. Additionally, we include a limit imposed on redshift due to detection of the afterglow in the R-band.
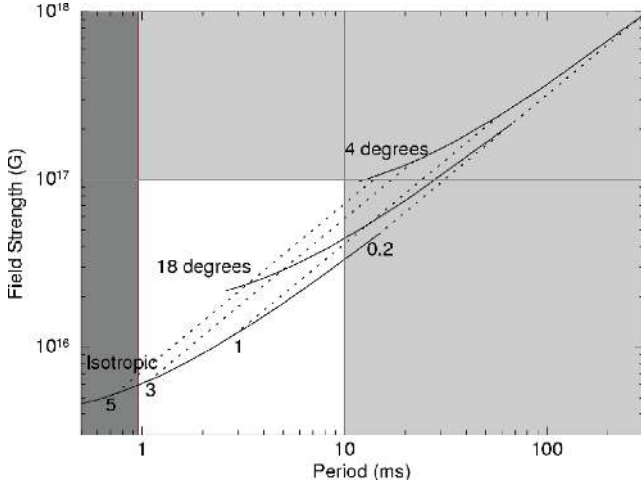
Figure 7. We show here the effect of beaming the emission of GRB 090515 assuming a mass of 1.4 $M_\odot$. Solid lines show isotropic solution and the solutions for the two beaming angles considered in Lyons et al. (2010). The dotted lines represent contours of equal redshift decreasing from left to right. The forbidden regions are as defined for Fig. 6(a).

for a binary merger progenitor (red curved dashed line):

$$B_{p,15}^2 > 10.8 T_{em,3}^{-2} L_{em,49}^{-1}, \tag{9}$$

$$P_{0,-3}^2 < 0.794 M_{1.4}^3 T_{em,3}^{-1} L_{em,49}^{-1}. \tag{10}$$

It has been suggested that the radii of proto-neutron stars may be as large as a few tens of kilometres (Ott et al. 2006), so in Fig. 6(c) we show the effect of increasing the radius, from 10 to 30 km, for a mass of 1.4 $M_\odot$, using the plateau luminosities and durations previously calculated for GRB 090515 assuming that it is at a range of redshifts. For larger radii, the unstable millisecond pulsar has to be at higher redshifts, and have a smaller magnetic field and larger period. As we have an *R*-band detection of the optical afterglow, we can place the upper limit $z \leq 5$ on the redshift.

In Fig. 7, we investigate the effect of the different beaming angles considered by Lyons et al. (2010) assuming a mass of 1.4 $M_\odot$. As the causality-forbidden region shown in Fig. 6(b and c) also depends on beaming angle we have reverted to using the regions defined by Lyons et al. (2010) for clarity. Up to this point, we have only considered isotropic emission and this shows beaming the emission would greatly affect the results obtained. Simulations have shown that a relativistic jet can be produced by a magnetar (Bucciantini et al. 2009). If the emission was beamed by 4°, the observations would not support the magnetar model. With a beaming angle of 18°, GRB 090515 would need a redshift of $1 < z < 5$ in order to satisfy the model and the constraints obtained by observing an optical afterglow. The more tightly the emission is beamed, the higher the redshift that the burst would need to be at in order to fit the magnetar model and this may explain why a host galaxy has not been identified.

5 CONCLUSIONS

GRB 090515 is a very unusual SGRB, as its low gamma-ray fluence would lead us to expect a significantly fainter X-ray light curve than observed at early times. Most importantly, the X-ray plateau followed by an extremely steep decay is very unusual, but may not be unique in the *Swift* sample. With a more sensitive detector,

the plateau observed by XRT may have instead been identified as part of the prompt emission and GRB 090515 might instead have been classified as an LGRB. Therefore, it poses interesting questions about the progenitor model and for the classification of other GRBs. In this paper, we have considered the two popular progenitor models for GRBs, collapsars and compact binary mergers.

GRB 090515 is the first SGRB with a fluence below 10^{-7} erg cm^{-2} with an observed optical afterglow at 1.75 h ($R = 26.4 \pm 0.1$), and this is the faintest detected optical afterglow for a GRB at that time.

We suggest that the simplest explanation for the unusual light curve of GRB 090515 is that it shows prolonged emission from an unstable millisecond pulsar, followed by an extremely steep decay when the millisecond pulsar collapses. Given the short duration of the GRB and the other properties, we favour the binary merger progenitor but cannot rule out a collapsar progenitor. For a collapsar progenitor, the proposed unstable millisecond pulsar with a spin period of 10 ms would have a magnetic field of $\sim 3 \times 10^{16}$ G at $z \sim 0.3$ and with a spin period of 1 ms the magnetic field would be $\sim 6 \times 10^{15}$ G at $z \sim 3.5$. The binary merger progenitor model gives a spin period of 10 ms and a magnetic field of $\sim 2.5 \times 10^{16}$ G at $z \sim 0.2$ to a spin period of 66 ms and a magnetic field of $\sim 4 \times 10^{15}$ G at $z \sim 4.4$. These values assume isotropic emission and a radius of 10 km.

REFERENCES

Antonelli L. A. et al., 2009, A&A, 507, L45
Barbier L. et al., 2005, GCN Circ., 4194, 1
Barthelmy S. et al., 2005b, GCN Circ., 3385, 1
Barthelmy S. et al., 2009a, GCN Circ., 9364, 1
Barthelmy S. et al., 2009b, GCN Circ., 9494, 1
Barthelmy S. D. et al., 2005a, Nat, 438, 994
Beardmore A. P., Evans P. A., 2009, GCN Circ., 9368, 1
Beardmore A. P. et al., 2009, GCN Circ., 9356, 1
Berger E., Kelson D., 2009, GCN Circ., 8934, 1
Berger E., Morrell N., Roth M., 2007, GCN, 7151, 1
Berger E., Cenko S. B., Fox D. B., Cucchiara A., 2009, ApJ, 704, 877
Bloom J. S., Frail D. A., Sari R., 2001, AJ, 121, 2879
Bloom J. S. et al., 2006, ApJ, 638, 354
Bucciantini N., Quataert E., Metzger B. D., Thompson T. A., Arons J., Del Zanna L., 2009, MNRAS, 396, 2038
Burrows D. N. et al., 2005, SSRv, 120, 165

Cenko S., Cobb B. E., Perley D. A., Bloom J. S., 2009, GCN Circ., 8933, 1
Costa E. et al., 1997, Nat, 387, 783
Cui X.-H., Aoi J., Nagataki S., Xu R.-X., 2010, preprint, (arXiv:1004.2302)
Dai Z. G., Lu T., 1998a, A&A, 333, L87
Dai Z. G., Lu T., 1998b, Phys. Rev. Lett., 81, 4301
Dai Z. G., Wang X. Y., Wu X. F., Zhang B., 2006, Sci, 311, 1127
Dall'Osso S., Stratta G., Guetta D., Covino S., De Cesare G., Stella L., 2010, preprint (arXiv:1004.2788)
Duncan R. C., Thompson C., 1992, ApJ, 392, L9
Eichler D., Livio M., Piran T., Schramm D. N., 1989, Nat, 340, 126
Evans P. A. et al., 2007, A&A, 469, 379
Evans P. A. et al., 2009, MNRAS, 397, 1177
Fan Y.-Z., Xu D., 2006, MNRAS, 372, L19
Fan Y. Z., Zhang B., Proga D., 2005, ApJ, 635, L129
Fenimore E. et al., 2005, GCN Circ., 4382, 1
Ferrero P. et al., 2007, AJ, 134, 2118
Gao W.-H., Fan Y.-Z., 2006, Chinese J. Astron. Astrophys., 6, 513
Gehrels N. et al., 2004, ApJ, 611, 1005
Gehrels N. et al., 2005, Nat, 437, 851
Godet O. et al., 2006, A&A, 452, 819
Hjorth J. et al., 2003, Nat, 423, 847
Hjorth J. et al., 2005a, Nat, 437, 859
Hjorth J. et al., 2005b, ApJ, 630, L117
Janiuk A., Moderski R., Proga D., 2008, ApJ, 687, 433
Klebesadel R. W., Strong I. B., Olson R. A., 1973, ApJ, 182, L85
Kocevski D. et al., 2010, MNRAS, 404, 963
Kumar P., Panaitescu A., 2000, ApJ, 541, L51
Lattimer J. M., Prakash M., 2004, Sci, 304, 536
Lattimer J. M., Schramm D. N., 1976, ApJ, 210, 549
Lattimer J. M., Prakash M., Masak D., Yahil A., 1990, ApJ, 355, 241
Levan A. J. et al., 2006, ApJ, 648, L9
Levan A. J., Tanvir N. R., Hjorth J., Malesani D., de Ugarte Postigo A., D'Avanzo P., 2009, GCN Circ., 154, 1
Li W., Chornock R., Filippenko A. V., 2009, GCN Circ., 9358, 1
Liang E. W. et al., 2006, ApJ, 646, 351
Lyons N., O'Brien P. T., Zhang B., Willingale R., Troja E., Starling R. L. C., 2010, MNRAS, 402, 705
Malesani D., de Ugarte Postigo A., Levan A. J., Tanvir N. R., Hjorth J., D'Avanzo P., 2009, GCN Circ., 156, 1
Markwardt C. et al., 2006, GCN Circ., 5330, 1
Mineo T. et al., 2005a, GCN, 4188, 1
Narayan R., Paczynski B., Piran T., 1992, ApJ, 395, L83
Nice D. J., Splaver E. M., Stairs I. H., Löhmer O., Jessner A., Kramer M., Cordes J. M., 2005, ApJ, 634, 1242
Norris J. P., Bonnell J. T., 2006, ApJ, 643, 266
Norris J. P., Gehrels N., Scargle J. D., 2010, ApJ, 717, 411
Nousek J. A. et al., 2006, ApJ, 642, 389
Nysewander M., Fruchter A. S., Pe'er A., 2009, ApJ, 701, 824

O'Brien P. T., Willingale R., Osborne J. P., Goad M. R., 2006, New J. Phys., 8, 121
Osborne J. P., Beardmore A. P., Evans P. A., Goad M. R., 2009, GCN Circ., 9367, 1
Ott C. D., Burrows A., Thompson T. A., Livne E., Walder R., 2006, ApJS, 164, 130
Pace C. J., Pearson R. L., Ward Moody J., 2009, GCN Circ., 9371, 1
Parsons A. et al., 2007, GCN Circ., 6656, 1
Perley D. A., Thoene C. C., Bloom J. S., 2007, GCN Circ., 6774, 1
Perley D. A., Bloom J. S., Modjaz M., Miller A. A., Shiode J., Brewer J., Starr D., Kennedy R., 2008, GCN Circ., 7889, 1
Perley D. A. et al., 2009a, ApJ, 696, 1871
Perley D. A., Kislak M., Ganeshalingam M., 2009b, GCN Circ., 9372, 1
Rowlinson A. et al., 2010, MNRAS in press (arXiv:1006.048)
Rujopakarn W., Schaefer B. E., Rykoff E. S., 2009, GCN Circ., 9357, 1
Sakamoto T., Breadmore A. P., 2009, GCN Circ., 9365, 1
Sakamoto T. et al., 2005, GCN Circ., 3305, 1
Sakamoto T. et al., 2007, GCN Circ., 6087, 1
Sakamoto T. et al., 2008, GCN Circ., 7761, 1
Sato G., Barthelmy S., 2007, GCN Circ., 6551, 1
Sato G. et al., 2005, GCN Circ., 3793, 1
Sato G. et al., 2007, GCN Circ., 6086, 1
Seigel M. H., Beardmore A. P., 2009, GCN Circ., 9369, 1
Soderberg A. M. et al., 2006, ApJ, 650, 261
Stanek K. Z. et al., 2003, ApJ, 591, L17
Starling R. L. C. et al., 2008, MNRAS, 384, 504
Stratta G. et al., 2007, A&A, 474, 827
Tody D., 1993, ASPC, 52, 173
Thompson T. A., 2007, Rev. Mex. Astron, 27, 80
Troja E. et al., 2007, ApJ, 665, 599
Ukwatta T. et al., 2008, GCN Circ., 7673, 1
Ukwatta T. N. et al., 2010, ApJ, 711, 1073
Usov V. V., 1992, Nat, 357, 472
Virgili F. J., Zhang B., O'Brien P., Troja E., 2009, preprint (arXiv:0909.1850)
Williams G. G., Updike A., Milne P. A., 2009, GCN Circ., 9360, 1
Willingale R. et al., 2007, ApJ, 662, 1093
Woosley S. E., Bloom J. S., 2006, ARA&A, 44, 507
Xin L. et al., 2010, preprint (arXiv:1002.0889)
Yi T., Liang E., Qin Y., Lu R., 2006, MNRAS, 367, 1751
Yu Y., Huang Y.-F., 2007, Chinese J. Astron. Astrophys., 7, 669
Yu Y.-W., Cheng K. S., Cao X.-F., 2010, ApJ, 715, 477
Zhang B., Mészáros P., 2001, ApJ, 552, L35
Zhang B., Fan Y. Z., Dyks J., Kobayashi S., Mészáros P., Burrows D. N., Nousek J. A., Gehrels N., 2006, ApJ, 642, 354
Zhang B. et al., 2009, ApJ, 703, 1696

This paper has been typeset from a T<small>E</small>X/L<small>A</small>T<small>E</small>X file prepared by the author.